



## RESEARCH ARTICLE OPEN ACCESS

## Soft 3D Lattice Iontronic Tactile Sensor

Jinhao Li<sup>1,2</sup>  | Qinghua Yu<sup>1</sup> | Zequn Shen<sup>1</sup> | Dong Wang<sup>1</sup> | Guoying Gu<sup>1,2</sup> <sup>1</sup>Robotics Institute and State Key Laboratory of Mechanical System and Vibration, School of Mechanical Engineering, Shanghai Jiao Tong University, Shanghai, China | <sup>2</sup>Shanghai Key Laboratory of Intelligent Robotics, Meta Robotics Institute, Shanghai Jiao Tong University, Shanghai, China**Correspondence:** Guoying Gu ([guguaying@sjtu.edu.cn](mailto:guguaying@sjtu.edu.cn))**Received:** 21 June 2025 | **Revised:** 12 August 2025 | **Accepted:** 22 August 2025**Funding:** This study was supported by National Key Research and Development Program of China (2024YFB4707504), National Natural Science Foundation of China (52025057, 524B2047), Science and Technology Commission of Shanghai Municipality (24511103400), and Xplorer Prize.**Keywords:** 3D printing hydrogel | human-machine interface | lattice structure | soft sensor | tactile sensing**ABSTRACT**

Designing soft electronic skins for tactile sensing facilitates natural human-machine communications. However, the nonlinear characteristics of electrical transductions and mechanics usually compromise precise tactile decoding and compliant interactions. In this work, we demonstrate a soft 3D-architected pressure sensor featuring a PEDOT:PSS-PVA hydrogel lattice encapsulated within an origami-inspired elastomeric framework. Our 3D lattice sensor leverages the ultracapacitive principle to achieve wide-range linearity (0–220 kPa), fast responses, and high-resolution detection under extreme loading. The proposed 3D configuration also enables linear compression behaviors within ~49.5% strain without sacrificing tissue-like compliance ( $E = 127\text{--}404$  kPa). Using this sensor as human-machine interfaces (HMIs), we facilitate accurate, timely, and stable pressure input for diverse signal waveforms in robotic teleoperation, as well as a deformable, intelligent fingertip for safely detecting soft tissue modulus. Our design provides a promising route to decode sophisticated tactile interactions by linearizing both electrical responses and mechanical behaviors.

**1 | Introduction**

Designing soft sensors to mimic biological skins facilitates natural haptic communications in telerobotics [1–3], virtual reality [4–6], and prostheses [7–9]. As a fundamental interaction modality, pressure forces give birth to diverse input paradigms for machine control [10–12], including click, sustained press and stepwise grading, as well as support biomechanical detections for natural systems such as palpation and elastography [13]. So far, numerous transduction mechanisms, including piezoresistive [14–16], triboelectric [17, 18], magnetic [19, 20] and capacitive [21, 22], have contributed to pressure sensing, achieving high sensitivity, low hysteresis, and mechanical robustness. Despite these advances, soft sensors usually exhibit nonlinear electrical transductions and mechanics due to the saturation effects of sensitivity and deformation [10]. These limitations compromise precise tactile decoding and conformal

contact, impeding seamless interactions between humans and robots.

Soft iontronics leverage the electrical double layer in elastic electronic-ionic contacts to detect applied pressure [23, 24]. This interfacial ultracapacitive mechanism has inspired various microstructure designs [25, 26], including pyramids, hemispheres, and grooves, to tailor electrical responses under loading. For example, the sequential deformation of gradient microstructure arrays progressively increases interfacial contacts, enabling broad-range linear responses (up to MPa) [27–29]. However, conventional 2.5D-architected designs inevitably cause the strain-stiffening behaviors in compressive mechanics [25]. This restriction complicates parameter calibration, dynamic monitoring and data processing in decoding diverse tactile interactions with position-controlled machines or robots. 3D structural engineering offers a promising route to program

This is an open access article under the terms of the [Creative Commons Attribution](https://creativecommons.org/licenses/by/4.0/) License, which permits use, distribution and reproduction in any medium, provided the original work is properly cited.

© 2025 The Author(s). *SmartBot* published by John Wiley & Sons Australia, Ltd on behalf of Harbin Institute of Technology.

compressive behaviors [30, 31]. Template-based conductive foams utilize porous compressibility to enhance deformation stroke but suffer from limited tunability and nonlinear behaviors [32–35]. The coupled electro-mechanical behavior and limited fabrication capabilities remain key challenges in designing soft iontronic sensors for pressure sensing.

Here, we present a 3D-architected soft iontronic sensor with linear electro-mechanical behaviors for decoding tactile interactions (Figure 1a). Our sensor comprises an origami-inspired elastomeric framework and an internal cryo-printed poly (3, 4-ethylenedioxythiophene): poly (styrene sulfonate)-poly (vinyl alcohol) (PEDOT:PSS-PVA) hydrogel lattice sandwiched by metal-plated fabrics. The as-formed capacitance enables wide-range linearity ( $0.022 \pm 0.002 \text{ kPa}^{-1}$  sensitivity within 0–220 kPa,  $R^2 = 0.993 \pm 0.005$ ), rapid responses, and high-resolution detection under extreme loading (0.007% FS at no load and 0.5% FS at 150 kPa). The proposed 3D configuration leverages controllable folding of the elastomeric framework to simultaneously achieve linear compression behaviors (within ~49.5% strain) and tissue-like compliance ( $E = 127\text{--}404 \text{ kPa}$ ). We further apply the 3D lattice (3DL) sensor as wearable HMIs and enable accurate, stable and timely control of sophisticated signal waveforms in robotic teleoperation by pressure-based tactile interactions. The integration with robotic end-effectors also demonstrates their capabilities to precisely and safely detect soft tissue elastic modulus as a deformable intelligent fingertip.

## 2 | Results and Discussion

### 2.1 | Design of Soft Iontronic Sensors With Linear Electro-Mechanical Behaviors

As shown in Supporting Information S1: Figure S1, we demonstrate typical structural configurations of soft iontronic sensors. The elastic interfaces between the bulk hydrogel and metal-plated electrodes transduce the compression into capacitance signals, where the surrounding framework facilitates the fast recovery of hydrogels after deformations. To eliminate nonlinear responses, we design PEDOT:PSS-PVA hydrogel lattices based on gyroid units in a size of  $8 \text{ mm} \times 8 \text{ mm} \times 6 \text{ mm}$  (Supporting Information S1: Figure S2). This hydrogel materials own the merits of inherent softness as well as mixed ionic and electronic conductivity, ensuring stable signals and consistent responses under deformations (Supporting Information S1: Figure S3 and S4). As a trade-off between the fingertip-like sensor size (~1 cm) and high-resolution printed features (~100  $\mu\text{m}$ ), we choose four gyroid units to form the hydrogel lattice. The designed lattices have tailorable volume percentages (defined as the ratio of the volume occupied by hydrogel materials to their total volume) to enlarge electronic-ionic contacts and resultant capacitances under progressive loading for wide-range linearity (Figure 1b). We further design origami-inspired elastomeric frameworks to replace the square spacer in the counterpart as the mechanical regulator (Supporting Information S1: Figure S5). Their controllable folding

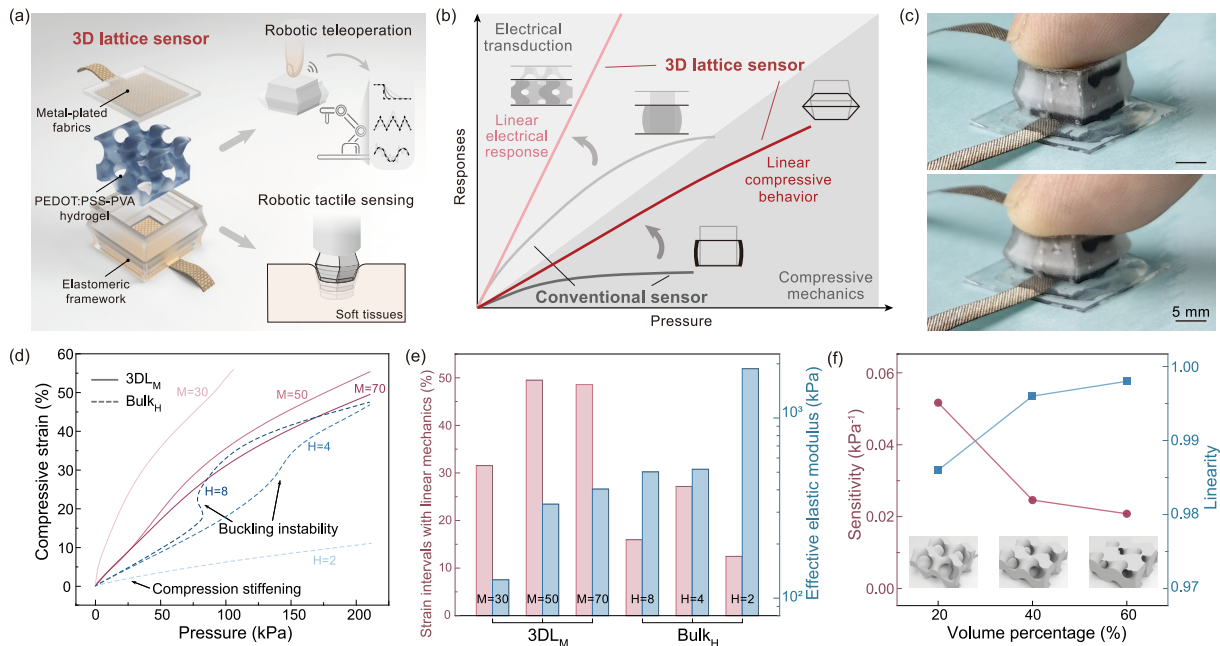


**FIGURE 1** | Design of the 3D-architected soft pressure sensor. (a) Schematic diagram on 3D lattice (3DL) sensors: structure designs and tactile interaction applications. (b) Schematic diagram of typical electro-mechanical responses of the 3DL sensor and the bulk sensor under loading. Conventional bulk sensors demonstrate the saturation effect on both compressive mechanics and electrical transduction. (c) Photographs of operating a 3DL sensor. (d) Compressive mechanics design of soft sensors. Square spacers with a ratio of height to thickness ( $H$ ) are labeled as “Bulk<sub>H</sub>”, whereas origami-inspired elastomeric frameworks with the hardness materials ( $M$ ) are labeled as “3DL<sub>M</sub>”, respectively. (e) Strain intervals with linear compressive mechanics and effective elastic modulus within strain intervals of varying elastomeric frameworks. (f) Hydrogel lattices with varying volume percentages affect the sensitivity and linearity of 3DL sensors.

deformations provide wide design spaces for linear compressive behaviors (Figure 1b). Finally, we encapsulate metal-plated fabrics and sandwiched hydrogels inside frameworks by silicone films to construct our 3DL sensors (Supporting Information S1: Figure S6 and Video S1). This enclosed construction prevents hydrogel dehydration and offers chamber-like mechanical support in operations. Combined with advanced printing techniques, our 3DL sensors have a size (10 mm × 10 mm × 6.5 mm) smaller than that of the human fingertip and exhibit mechanical reliability in repeating compressions (Figure 1c).

We first design the compressive mechanics of soft 3DL sensors. Conventional square spacers in bulk sensors commonly exhibit compressive strain-stiffening behaviors and high elastic modulus ( $E > 1$  MPa). One straightforward route is increasing the aspect ratio of spacers (i.e., the ratio of spacer height to thickness, defined as  $H$ ) to reduce structure stiffness but cause buckling instability in compression. On the contrary, our origami-inspired elastomeric frameworks enable high linearity ( $R^2 = 0.98$ ) in ~49.5% compressive strain (> 2 times longer than the counterpart) (Figure 1d,e), covering the full scale of pressure detection. Notably, the strain intervals with linear mechanics, as shown in Figure 1e, are calculated from the strain–pressure curves (Figure 1d), using a linearity of 0.98 as the standard. We further regulate the hardness of composed materials (defined as  $M$  with the unit of kilopascal) for frameworks and achieve tissue-like effective elastic modulus ( $E = 127$ – $404$  kPa), providing mechanical compatibility for wearable HMIs. Herein, we use the label “Bulk<sub>H</sub>” for square spacers with a ratio of height to thickness ( $H$ ) and the label “3DL<sub>M</sub>” for origami-inspired elastomeric frameworks with the hardness materials ( $M$ ), respectively. We next cryo-print PEDOT:PSS-PVA hydrogel lattices that have differential volume percentages (20%, 40%, and 60%). The results demonstrate that low-volume-percentage lattices decrease the signal baseline under no loading and thus enhance the sensitivity while weakening the elastic recovery after loading and causing hysteresis behaviors (Supporting Information S1: Figure S7). As a trade-off between sensitivity and linearity, we choose the volume percentage of 40% for PEDOT:PSS-PVA hydrogel lattices (Figure 1f).

## 2.2 | Characterizations on Sensing Performances of Soft 3DL Sensors

Next, we characterize the sensing performances of soft iontronic sensors. As shown in Figure 2a, conventional bulk sensors exhibit typical zig-zag electrical responses with piecewise linearity (classified into 3 intervals with the linearity of 0.99). The limited sensitivity under low- and high-pressure (0–43 kPa or 78–220 kPa) covers 84% measuring range, whereas our sensor demonstrates high linearity ( $R^2 = 0.993 \pm 0.005$ ) over a broad pressure range (0–220 kPa) (Figure 2b). To characterize the mechanism of linear electrical response, we in situ monitor the deformation behaviors under compressive strain of 25% and 50% using X-ray computed tomography (Figure 2c and Supporting Information S1: Figure S8). The results show that the compression causes progressive collapsing of the hydrogel lattice and a

synchronous expansion of the contact area between the hydrogel lattice and electrodes. The contact area increases by 24.1% and 49.5% under the compressive strain of 25% and 50%, respectively. Notably, this rising contact area facilitates the formation of more electron–ion pairs at interfaces and enables a growing capacitance for iontronic pressure sensing. We further perform the finite element analysis to investigate the increasing behaviors of the contact area between the hydrogel lattice and the electrode. As shown in Figure 2d, the relative variation of the interface contact area increases linearly with the compressive strain ( $R^2 = 0.99$ ). The results prove that the linear electrical responses (Figure 2a) are attributed to the linear expansion of the contact area between the gradually collapsing hydrogel lattice and electrodes under pressure. This mechanism also enables an order of magnitude increase in sensitivity ( $0.022 \pm 0.002$  kPa<sup>-1</sup>) over lattice-based parallel-plate capacitors [36]. We further investigate the response capabilities of our 3DL sensors under extreme loading. For example, after applying a tiny nut (0.15 g weight), the sensor demonstrates an instant detection containing clear rising and falling edges (Figure 2e), exhibiting a limit of detection (LOD) of ~15 Pa. The rise time and fall time are defined as the time of the transition process from 10% to 90% of its steady-state amplitude. We also characterize the detection resolution of the sensor under high preloading (150 kPa), and the results show that even a slight stepwise loading (~1 kPa) can be clearly reflected in the capacitance signals (Figure 2f). The high-resolution detection under extreme loading (0.007% FS at no load and 0.5% FS at 150 kPa) enables the capture of slight vibrations in dynamic tactile interactions. We also evaluate the responsive stability and signal reliability under loading. As shown in Figure 2g, our 3DL sensor demonstrates segment stability when loaded with the step-up pressures of 20 kPa to a maximum of 70 kPa and then unloaded to the initial state without obvious capacitance creep. Long-term cyclic tests at a pressure of 40 kPa further reveal the stable electrical responses and mechanical deformations, without observing significant degradation in sensing performance upon 4000 loading-unloading cycles (Figure 2h). Compared with previous works (Supporting Information S1: Figure S9 and Table S1) [23, 33, 34, 36–42], our 3DL sensors demonstrate outstanding linear electro-mechanical behaviors and rapid yet precise detection capabilities.

## 2.3 | Wearable Human-Machine Interfaces for Robotic Teleoperation

Robotic teleoperation through HMIs promises to augment human capabilities safely in hazardous or inaccessible environments. As a typical complicated electromechanical process, wearable teleoperation contains touch actions in mechanics and signal transductions in electronics. Typical demonstrations are usually achieved by comparing the amplitude of sensing signals with default thresholds to implement switch commands. It is still challenging to reproduce complex functions of traditional rigid controllers like impulsive control and proportional control. Herein, linear electromechanical behaviors of 3DL sensors facilitate natural tactile interaction and precise signal decoding for sophisticated input modalities (Figure 3a). We first recruit four participants to use pressure sensors as soft tactile buttons and leverage the pressure input to track diverse signal

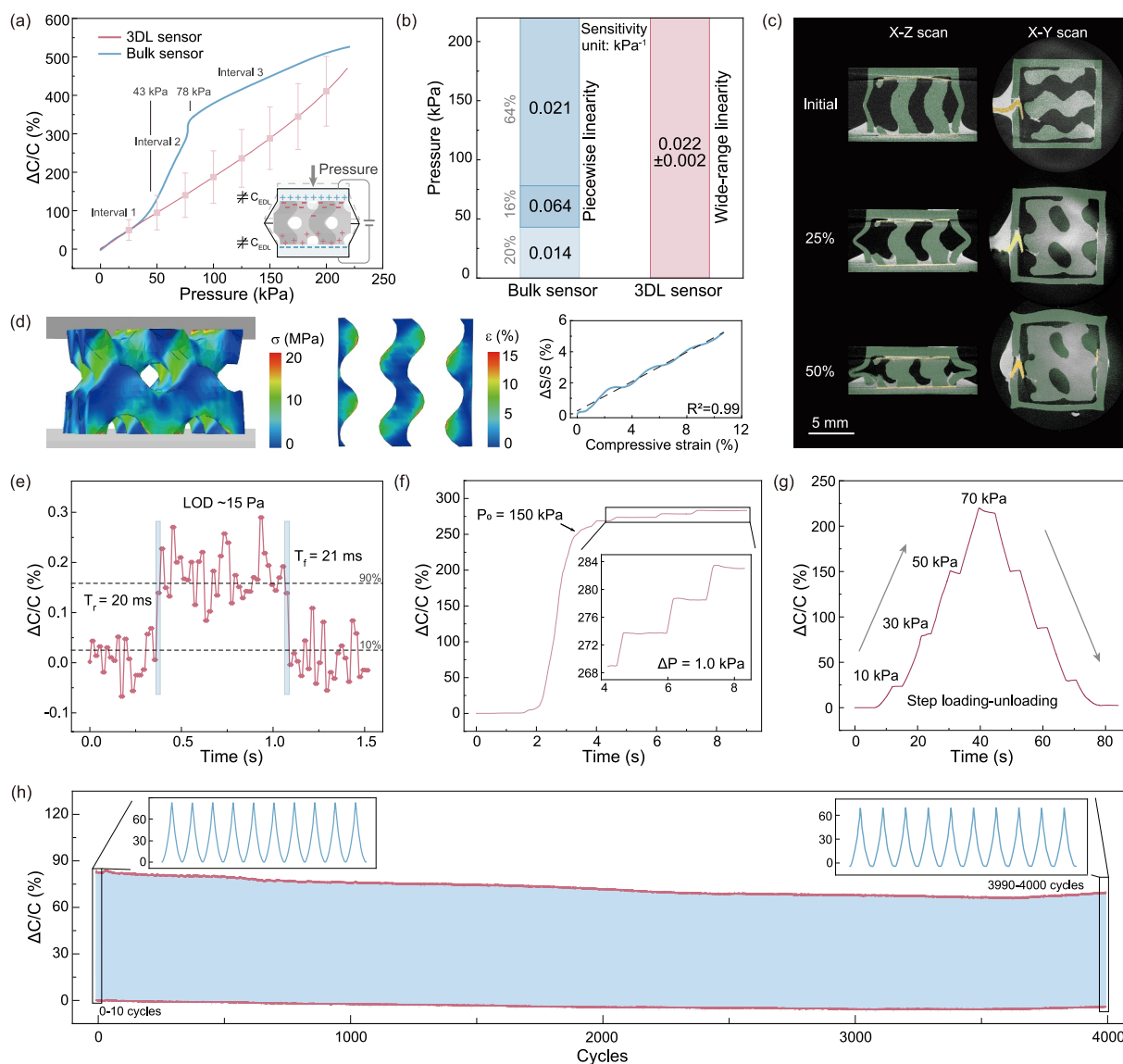


**FIGURE 2** | Characterizations of the 3D-architected soft pressure sensor. (a) Electrical responses of the 3DL sensor and the bulk sensor under loading. The insert illustrates the ultracapacitive mechanism in our 3DL sensors. Error bars are  $\pm$  Sd for  $n = 3$ . (b) Comparisons on the sensitivity over a broad pressure range. The standard deviation is calculated based on three independent samples. (c) In situ observation of 3DL sensors under differential compressive strain. Metal-plated fabrics are marked in yellow, and hydrogel lattices and elastomeric frameworks are marked in green. (d) Finite element analysis on compressive mechanics and electrode-hydrogel interfacial area,  $S$ , of 3DL sensors. (e) Typical transient response of the 3DL sensor, exhibiting a low limit of detection ( $\sim 15$  Pa) and instant response. (f) Detection resolution of sequential subtle pressures under high preloading by using a 3DL sensor. (g) Capacitance responses of the 3DL sensor under a series of step-up and step-down loading. (h) Cycling stability at the pressure of 40 kPa (4000 cycles). The insets show the capacitance response in the first 10 cycles and the last 10 cycles.

waveforms (Video S2). During the experiments (Figure 3b), the subjects are informed to lightly touch and firmly press sensors to calibrate the normalization bounds (typically 5–100 kPa), and then track three waveforms (step, ramp, and sine functions) by pressure input. These trials are performed with a computer timer to guide subjects to execute the entire experiment, and capacitance data are collected and decoded in real time.

As shown in Supporting Information S1: Figure S10, the average tracking performances demonstrate that the pressure input by using 3DL sensors has a higher accuracy and less fluctuation than that by bulk sensors. We further characterize the shape fidelity, repeatability, and hysteresis of tracking signals for

comprehensive comparison (Figure 3c–e). Using 3DL sensors, the average deviations of tracking signals decrease by 64.1%, 28.6% and 47.6% on step, ramp and sine functions, respectively, with being statistically significant ( $p < 0.001$ ) (Figure 3c). We further calculate the standard deviations among the sequential tracking signals in repeated operations, and the results show our 3DL sensors enable more consistent pressure input and significantly reduce the repeatability errors by 63.9%, 20.6% and 38.4% on different waveforms ( $p < 0.001$ ) (Figure 3d). We also perform the hysteresis performance of tracking signals. Notably, we consider the step function's tracking process as a first-order system and fit it using the function  $y = 1 - e^{-t/\tau}$  to derive the time constant  $\tau$  for the delay time. Otherwise, we determine the delay

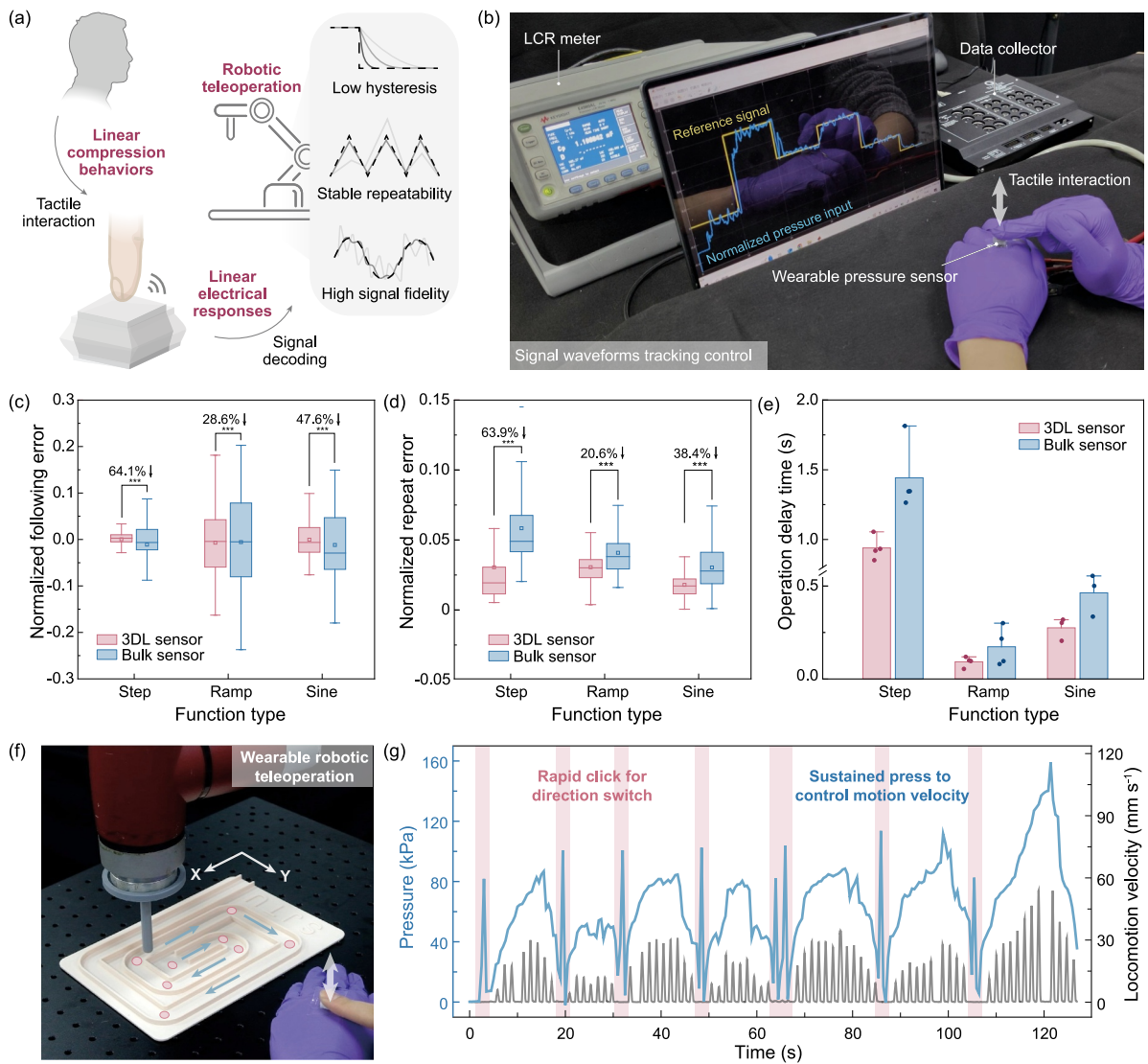


**FIGURE 3** | Wearable human-machine interfaces for robotic teleoperation based on 3DL sensors. (a) Schematic diagram of tactile interactions for robotic teleoperation, enhanced by the linear electro-mechanical behaviors of 3DL sensors. (b) Photograph of a wearable 3DL sensor for pressure input (c–e) Performance comparisons on tracking different waveforms: (c) Normalized tracking errors. \*\*\* means  $p < 0.001$  (Wilcoxon signed-rank test). (d) Normalized repeat errors. \*\*\* means  $p < 0.001$  (Wilcoxon signed-rank test). (e) Operation delay time. (f) Photograph of wearable robotic teleoperation by pressure input. (g) Detected pressure by the 3DL sensor and robotic locomotion velocity during the targeted labyrinth task. Error bars are  $\pm$  Sd for  $n = 4$ .

time by shifting the reference signal along the time axis and recording the time shift corresponding to the maximum cross-correlation coefficient. The results demonstrate that the 3DL sensors facilitate reduced signal delays by 34.8%, 46.7% and 40.6% to their counterparts (Figure 3e). These capabilities of 3DL sensors promise to expand the interaction paradigm for robotic teleoperation based on soft sensors. For example, we preprogram the industrial controller to automatically identify the pressure input at HMIs into rapid clicks and sustained presses, which remotely control the motion direction and feed velocity of an industrial robot, respectively (Figure 3f). Thus, the subject can teleoperate the robot to go through a planar labyrinth along the target trajectory with adaptive velocities (Figure 3g and Video S3), balancing rapid mobility and agile locomotion.

## 2.4 | Deformable Intelligent Fingertip for Safely Detecting Soft Tissue Modulus

Intelligent robotic fingertips are expected to identify physical properties such as the hardness/softness of the touched objects through tactile interactions. However, typical nonlinear electro-mechanical coupling behaviors of soft sensors usually require pre-trained machine-learning networks for information decoding. Herein, 3DL sensors enable safe and gentle touch for data collection and simplified processing for modulus detection. We integrate the 3DL sensor onto a position-controlled robotic end-effector (Figure 4a). In typical indentation tests (Supporting Information S1: Figure S11), we can build the load-displacement relationship to solve the elastic modulus. The contact forces

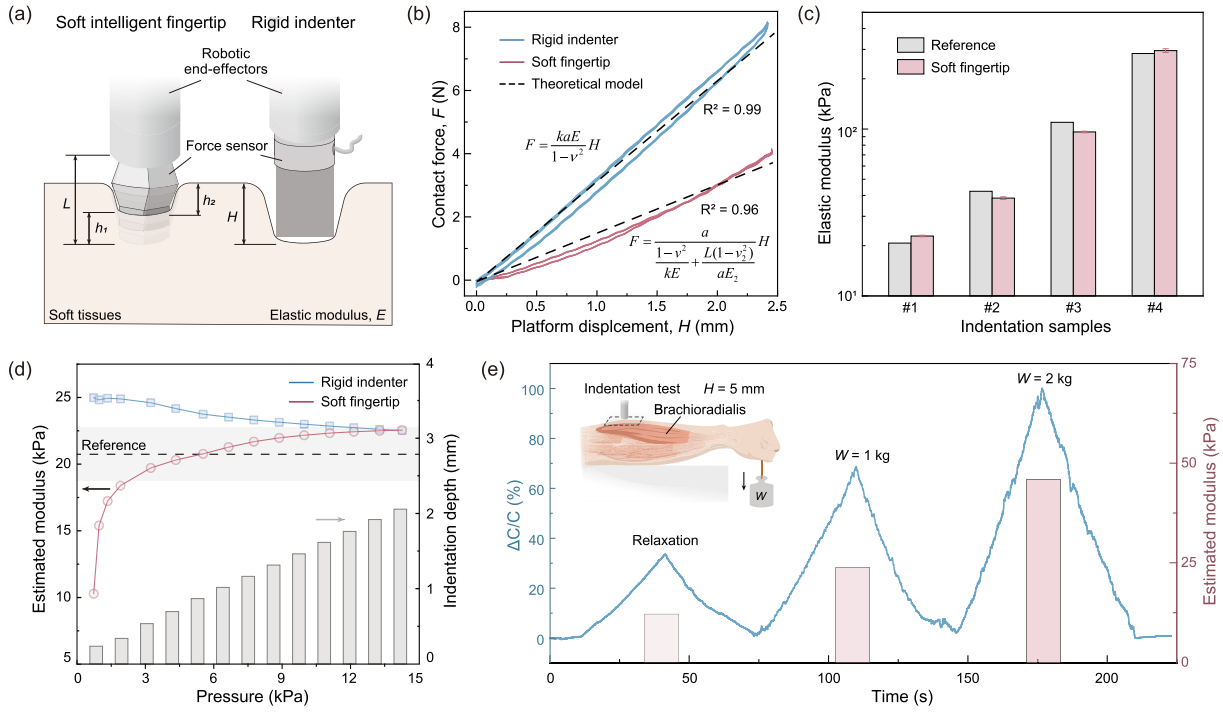


**FIGURE 4** | Deformable intelligent fingertip for safely detecting soft tissue modulus. (a) Schematic diagram of indentation tests by using a 3DL sensor-based intelligent fingertip and a conventional rigid indenter. (b) Typical compression behaviors and theoretical models in indentation tests for soft and rigid indenters.  $K$  shape factor,  $\nu$  Poisson's ratio,  $a$  square side length. The contact forces are derived from the rigid force sensor and the inverse solution of soft 3DL sensors, respectively. (c) The elastic modulus detection of varying soft samples. Error bars are  $\pm Sd$  for  $n = 5$ . (d) The calculated elastic modulus converges with the increasing indentation depth and pressure. Soft intelligent fingertip facilitates modulus detection under gentle touch. (e) Indentation tests for monitoring tissue modulus at the brachioradialis muscle under isometric contractions.

between a rigid indenter and samples,  $F$ , measured by a force cell, can be expressed as follows:

$$F = \frac{kaE}{(1-\nu^2)}h_1, \quad (1)$$

where  $k$  and  $a$  are the shape factor and side length of the indenter, and  $h_1$  is the indentation depth (equal to the platform displacement  $H$  for rigid indenters). Here, we simplify the soft samples to be measured as an elastic deformed semi-infinite solids, and adopt the shape factor  $k = 2.3$  for square-shaped indenters [43].  $E$  and  $\nu$  are the elastic modulus and Poisson's ratio of soft samples to be measured.

Using a 3DL sensor, the intelligent fingertip compresses and deforms during contact with soft samples; thus, the platform displacement  $H$  can be expressed as follows:

$$H = h_1 + h_2, \quad (2)$$

where  $h_1$  and  $h_2$  are the indentation depth and compressive deformation of 3DL sensors and can be expressed as follows:

$$h_1 = \frac{(1-\nu^2)}{kaE}F, \quad (3)$$

$$h_2 = \frac{L(1-\nu_2^2)}{a^2E_2}F, \quad (4)$$

where  $E_2$  and  $\nu_2$  are the elastic modulus and Poisson's ratio of 3DL sensors, and  $L$  is the height of 3DL sensors. The radial

deformation of 3DL sensors can be ignored because the contact is constrained to their ends, and the load-displacement relationship for soft fingertips can be expressed as follows:

$$F = \frac{a}{\frac{(1-\nu^2)}{kE} + \frac{L(1-\nu_2^2)}{aE_2}}H, \quad (5)$$

where the contact forces between the 3DL sensor and samples can be decoded by its capacitance signals. Thus, we can estimate the elastic modulus by fitting load-displacement curves (Figure 4b and Video S4). We characterize varying soft samples with differential moduli ( $E = 20.7, 42.4, 109.7, \text{ and } 283.6$  kPa). The results demonstrate that the soft intelligent fingertip enables accurate estimations with an average error of 8.9% (Figure 4c,d), where its conformal contact allows rapid convergence in solving modulus under a biocompatible low pressure ( $< 8$  kPa) [44, 45]. We also conduct the indentation tests at the brachioradialis muscle under different levels of isometric contractions, and the intelligent fingertip detects a step-up elastic modulus under the increasing wrist extension load (Figure 4e). This soft intelligent fingertip will enrich the tactile perception capabilities for position-controlled robots.

## 2.5 | Discussion

This work introduces a design to linearize both electrical responses and compressive mechanics for iontronic sensors, facilitating tactile decoding at human-robot interfaces. Despite the above demonstrations, several aspects remain in need of

improvement. First, the strategy that leverages the deformation of 3D structures to change interfacial capacitance weakens the high sensitivity compared to microstructured iontronic sensors. It is foreseeable that further designs on hydrogels with high ionic conductivity and hierarchical structures will eliminate this issue in future research [46, 47].

Cryogenic printing and origami-structured molding techniques are presented in this work, allowing for 3D-architected iontronic sensors with tailored properties. However, in current experiments, each part of the device is manufactured separately and assembled manually. This lack of high-throughput mass production limits its cost, consistency, and industrial integration. One promising approach is to develop multimaterial multinozzle printing inside a compact temperature-controlled space, utilizing universal phase transition or thermal polymerization of polymers. This development of a continuous fabrication technique will also facilitate robust interfaces for system integration.

In this study, we use elastomeric frameworks for the encapsulation of hydrogel lattices. However, current hydrogels are commonly affected by varying temperature, dehydration or humidity due to the water vapor permeability [48]. Although temporary inference can be decoupled by an additional calibration sensor (Supporting Information S1: Figure S12), this phenomenon may also disturb the ionic migration and cause performance degradation in long-term cycling (typically < 5000 cycles), limiting practical robotic applications in harsh environments. Herein, further introduction of hydrophobic elastomers, water-retaining agents and tethered supported bilayers will facilitate stable sensing with robustness.

In practical applications, oblique compression, shear, or bending loads may influence the interfacial contact and robust perception for 3D-architected sensors (Supporting Information S1: Figure S13), where structural bending stiffness requires detailed designs [49]. Inadequate interfacial contact also exacerbates the boundary effect of lattice structures and affects the detection accuracy upon slight touch.

### 3 | Conclusion

In this study, we propose a soft 3D lattice iontronic sensor harnessing linear electro-mechanical behaviors for precise tactile sensing and natural interactions between humans and robots. Combining with cryogenic printing techniques, we facilitate origami-inspired elastomeric frameworks filled with PEDOT:PSS-PVA hydrogel lattices for iontronic pressure sensing. Our 3D-architected ultracapacitive designs simultaneously achieve wide-range linearity in electrical responses ( $R^2 = 0.993 \pm 0.005$  within 0–220 kPa) and compressive mechanics ( $R^2 = 0.98$  within ~49.5% strain) as well as rapid yet high-resolution detection. Using as wearable HMIs, we facilitate accurate, stable, and timely control of sophisticated signal waveforms in robotic teleoperation by pressure input. We further integrate the sensors with robotic end-effectors and achieve the precise and safe detection of soft tissue elastic modulus as a deformable intelligent fingertip. Our design

promises decoding human–machine interactions by reconciling electrical responses and mechanical behaviors.

## 4 | Experimental Methods

### 4.1 | Fabrication of Elastomeric Frameworks

As shown in Supporting Information S1: Figure S6 and Video S1, we first fabricated commercial metal-plated fabrics (Shenzhen Changdasheng Electronics Co. Ltd.) into customized electrode patterns by laser cutting (VLS 3.50, Universal Laser Systems), and glued them onto a casting mold as one electrode for sensors. The casting mold was designed into three parts, including a drum-like convex platform and two clamps, for the origami-inspired framework with thin-walled and hollow features. The designed mold was then fabricated by a commercial 3D printer (Bambu Lab X1) and assembled based on its mortise-and-tenon structures before casting. To obtain the silicone framework, we mixed the matrix and curing agent of polydimethylsiloxane (PDMS, Sylgard 184, Dow Corning Corp.) in a 10:1 weight ratio. The PDMS precursor was degassed in a vacuum chamber for 15 min to remove air bubbles and then poured onto designed casting molds, followed by curing at 80°C for 4 h. We also tailored elastomeric frameworks with polyurethane materials that have differential hardness (Shore A 30, 50, and 70) to investigate their influences on compressive mechanics.

### 4.2 | Cryogenic Printing of Hydrogel Lattices

The PEDOT: PSS-PVA hydrogel lattice was cryo-printed by our previously proposed approach [50]. We re-dispersed PEDOT: PSS nanofibrils (Orgacon Dry) in a deionized water-dimethyl sulfoxide (DMSO,  $\geq 99\%$ , Aladdin Reagent Co. Ltd) mixture (85:15 v/v) and thoroughly mixed with PVA inks (10 wt%, Mw = 146,000–186,000, > 99% hydrolyzed, Sigma-Aldrich) with a syringe filter (30  $\mu\text{m}$ ) to prepare PEDOT:PSS-PVA inks. The mass ratio of 7% PEDOT: PSS solution to 10% PVA solution is 1:4. The mixed PEDOT:PSS-PVA inks were then extruded using a custom-made 3D printer onto a Peltier plate at the varying temperature of  $-7^\circ\text{C}-0.2^\circ\text{C min}^{-1}$ . The frozen structures were then immersed in a cryogenic aqueous cross-linking bath ( $-5^\circ\text{C}$ ) for 16 h, containing 0.2 M hydrochloric acid, 0.01 M Glutaraldehyde (25% in  $\text{H}_2\text{O}$ , Macklin Biochemical Technology Co., Ltd), and 5 M anhydrous ethanol. The obtained PEDOT: PSS-PVA hydrogel was washed in deionized water several times.

### 4.3 | Assembly of Soft Iontronic Sensors

Finally, the customized electrode was adhered to silicone films and assembled with an elastomeric framework and a hydrogel lattice by using silicone adhesion (Ecoflex 00–35 fast, A:B = 1:1). The whole 3DL sensor was baked at 60°C for 5 min to cure fully. The bulk sensor was fabricated similarly, whereas the bulk hydrogels were cast in a cuboid mold at  $-20^\circ\text{C}$  and then cryogenic cross-linked in the same condition.

#### 4.4 | Mechanical Characterizations

The mechanical characterizations were conducted on universal mechanical testing equipment (Instron 68SC-2, USA) at a constant crosshead speed of 15 mm min<sup>-1</sup>. The application of high preloading was carried out by manually releasing a free sliding platform. To prepare soft samples for indentation tests, we cast four kinds of silicone (Ecoflex 10, Ecoflex 00–35 fast, Dragon skin 10, and Dragon skin 30, A:B = 1:1) into blocks (50 mm × 50 mm × 50 mm) and cured at 80°C for 4 h. A computer-controlled stepping motor-driven stage (HST-200, OptoSigma Inc.) was applied to conduct the indentation tests, and a force gauge (LSB200, Futek Advanced Sensor Technology Inc.) was further equipped to measure the contact forces for conventional rigid indenters.

#### 4.5 | Electrical Characterizations

The electrical signals were measured by a precise LCR (inductance-capacitance-resistance) meter (E4980AL, Keysight Technologies Inc.) with the sample rate at 1 kHz and collected by a data acquisition board (Quenser Inc.). The capacitance signals of soft iontronic sensors were processed by using MATLAB (The MathWorks Inc.) and conducted significance analysis in Origin (The OriginLab Corp.).

#### 4.6 | Significance Analysis

In significance analysis, we first conducted skewness calculation and symmetry assessment, incorporating outlier detection using Z-scores for tracking signals of step functions. Then, we conducted Wilcoxon signed-rank tests on the decoding pressure data for statistical significance testing with directional hypothesis determination based on median differences, considering the volunteers performed identical tasks under matched conditions.

#### 4.7 | X-Ray Computed Tomography

The compression behaviors of 3DL sensors were in situ imaged by using an Xradia 520 Versa CT scanner (Zeiss, Germany). The reconstruction was conducted using the software Dragonfly.

#### 4.8 | Compressive Mechanics Simulations

The finite element analysis was performed by using the software Abaqus. The mechanics simulation was carried out by using the linear elastic model, and the modulus of the hydrogel lattice was set as 75.9 kPa. Self-contact and mutual contact were considered, whereas the coefficient of friction was set as 0.2. The 10-node quadratic tetrahedron element C3D10 M was used. Refined meshes were adopted to ensure computational accuracy. The texture of metal-plated fabrics and the slight solvent leakage of highly compressed hydrogels are neglected to simplify the simulation.

#### 4.9 | Participant Recruitments

All experiments were conducted in accordance with the Declaration of Helsinki and approved by the Institutional Review Board for Human Research Protections of Shanghai Jiao Tong University.

#### Author Contributions

**Jinhao Li:** conceptualization, writing – original draft, writing – review and editing, methodology, investigation, funding acquisition. **Qinghua Yu:** data curation, writing – review and editing, visualization, investigation. **Zequn Shen:** visualization, data curation, writing – review and editing, investigation. **Dong Wang:** writing – review and editing, validation, formal analysis. **Guoying Gu:** conceptualization, supervision, writing – original draft, writing – review and editing, funding acquisition.

#### Conflicts of Interest

The authors declare no conflicts of interest.

#### Data Availability Statement

All data needed to evaluate the conclusions are presented in the paper, its Experimental Methods, and Supplementary Information. The original videos and data are available from the corresponding authors on reasonable request.

#### References

1. Z. Shen, Z. Zhang, N. Zhang, et al., “High-Stretchability, Ultralow-Hysteresis Conducting Polymer Hydrogel Strain Sensors for Soft Machines,” *Advanced Materials* 34, no. 32 (2022): 2203650, <https://doi.org/10.1002/adma.202203650>.
2. J. Park, Y. Lee, S. Cho, et al., “Soft Sensors and Actuators for Wearable Human–Machine Interfaces,” *Chemical Reviews* 124, no. 4 (2024): 1464–1534, <https://doi.org/10.1021/acs.chemrev.3c00356>.
3. C. Wei, W. Lin, S. Liang, et al., “An All-In-One Multifunctional Touch Sensor With Carbon-Based Gradient Resistance Elements,” *Nano-Micro Letters* 14, no. 1 (2022): 131, <https://doi.org/10.1007/s40820-022-00875-9>.
4. Z. Sun, M. Zhu, X. Shan, and C. Lee, “Augmented Tactile-Perception and Haptic-Feedback Rings as Human-Machine Interfaces Aiming for Immersive Interactions,” *Nature Communications* 13, no. 1 (2022): 5224, <https://doi.org/10.1038/s41467-022-32745-8>.
5. J. Yin, R. Hinchet, H. Shea, and C. Majidi, “Wearable Soft Technologies for Haptic Sensing and Feedback,” *Advanced Functional Materials* 31, no. 39 (2020): 2007428, <https://doi.org/10.1002/adfm.202007428>.
6. Y. Liu, C. Yiu, Z. Song, et al., “Electronic Skin as Wireless Human-Machine Interfaces for Robotic VR,” *Science Advances* 8, no. 2 (2022): eabl6700, <https://doi.org/10.1126/sciadv.abl6700>.
7. H. Xu, G. Chai, N. Zhang, and G. Gu, “Restoring Finger-Specific Tactile Sensations With a Sensory Soft Neuroprosthetic Hand Through Electrotactile Stimulation,” *Soft Science* 2, no. 4 (2022): 19, <https://doi.org/10.20517/ss.2022.17>.
8. J. Li, J. Cao, B. Lu, and G. Gu, “3D-Printed PEDOT:PSS for Soft Robotics,” *Nature Reviews Materials* 8, no. 9 (2023): 604–622, <https://doi.org/10.1038/s41578-023-00587-5>.
9. C. Zhao, J. Park, S. E. Root, and Z. Bao, “Skin-Inspired Soft Bioelectronic Materials, Devices and Systems,” *Nature Reviews Bioengineering* 2, no. 8 (2024): 671–690, <https://doi.org/10.1038/s44222-024-00194-1>.

10. R. Chen, T. Luo, J. Wang, et al., "Nonlinearity Synergy: An Elegant Strategy for Realizing High-Sensitivity and Wide-Linear-Range Pressure Sensing," *Nature Communications* 14, no. 1 (2023): 6641, <https://doi.org/10.1038/s41467-023-42361-9>.
11. L. Liu, S. Yu, Y. Xu, et al., "Dynamically Reversible Filament Networks Enabling Programmable In-Sensor Memory for High-Precision Neuromorphic Interactions," *Advanced Functional Materials* (2025): 2504456, <https://doi.org/10.1002/adfm.202504456>.
12. Z. Shen, J. Ren, N. Zhang, J. Li, and G. Gu, "Hierarchically-Interlocked, Three-Axis Soft Iontronic Sensor for Omnidirectional Shear and Normal Forces," *Advanced Materials Technologies* 10, no. 5 (2024): 2401626, <https://doi.org/10.1002/admt.202401626>.
13. D. G. Raitt, M. Huseynov, S. Homer-Vanniasinkam, H. A. Wurde-mann, and S.-A. Abad, "Soft-Tipped Sensor With Compliance Control for Elasticity Sensing and Palpation," *IEEE Transactions on Robotics* 40 (2024): 2430–2441, <https://doi.org/10.1109/tro.2024.3371691>.
14. H. Xu, Y. Rong, J. Ren, et al., "A Learning-Based Sensor Array for Untethered Soft Prosthetic Hand Aiming at Restoring Tactile Sensation," *Advanced Intelligent Systems* 6, no. 10 (2023): 2300221, <https://doi.org/10.1002/aisy.202300221>.
15. Y. Li, W. Zhang, C. Zhao, et al., "Breaking the Saturation of Sensitivity for Ultrawide Range Flexible Pressure Sensors by Soft-Strain Effect," *Advanced Materials* 36 (2024): 2405405, <https://doi.org/10.1002/adma.202405405>.
16. J. Su, H. Zhang, H. Li, et al., "Skin-Inspired Multi-Modal Mechanoreceptors for Dynamic Haptic Exploration," *Advanced Materials* 36, no. 21 (2024): 2311549, <https://doi.org/10.1002/adma.202311549>.
17. S. Liu, Y. Li, W. Guo, et al., "Triboelectric Nanogenerators Enabled Sensing and Actuation for Robotics," *Nano Energy* 65 (2019): 104005, <https://doi.org/10.1016/j.nanoen.2019.104005>.
18. Y. Liu, L. Wang, L. Zhao, et al., "Thin, Skin-Integrated, Stretchable Triboelectric Nanogenerators for Tactile Sensing," *Advanced Electronic Materials* 6, no. 1 (2019): 1901174, <https://doi.org/10.1002/aelm.201901174>.
19. Y. Yan, Z. Hu, Z. Yang, et al., "Soft Magnetic Skin for Super-Resolution Tactile Sensing With Force Self-Decoupling," *Science Robotics* 6, no. 51 (2021): eabc8801, <https://doi.org/10.1126/scirobotics.abc8801>.
20. Y. Yan, A. Zermane, J. Pan, and A. Kheddar, "A Soft Skin With Self-Decoupled Three-Axis Force-Sensing Taxels," *Nature Machine Intelligence* 6, no. 11 (2024): 1284–1295, <https://doi.org/10.1038/s42256-024-00904-9>.
21. G. Gu, N. Zhang, H. Xu, et al., "A Soft Neuroprosthetic Hand Providing Simultaneous Myoelectric Control and Tactile Feedback," *Nature Biomedical Engineering* 7, no. 4 (2021): 589–598, <https://doi.org/10.1038/s41551-021-00767-0>.
22. X. Sheng, Z. Qin, H. Xu, X. Shu, G. Gu, and X. Zhu, "Soft Ionic-Hydrogel Electrodes for Electroencephalography Signal Recording," *Science China Technological Sciences* 64, no. 2 (2020): 273–282, <https://doi.org/10.1007/s11431-020-1644-6>.
23. Z. Shen, X. Zhu, C. Majidi, and G. Gu, "Cutaneous Ionogel Mechanoreceptors for Soft Machines, Physiological Sensing, and Amputee Prostheses," *Advanced Materials* 33, no. 38 (2021): 2102069, <https://doi.org/10.1002/adma.202102069>.
24. Y. Chang, L. Wang, R. Li, et al., "First Decade of Interfacial Iontronic Sensing: From Droplet Sensors to Artificial Skins," *Advanced Materials* 33, no. 7 (2020): 2003464, <https://doi.org/10.1002/adma.202003464>.
25. Y. Wang, K. Jia, and Z. Suo, "Non-Faradaic Junction Sensing," *Nature Reviews Materials* 10, no. 3 (2024): 176–190, <https://doi.org/10.1038/s41578-024-00755-1>.
26. Z. Shen, F. Chen, X. Zhu, K.-T. Yong, and G. Gu, "Stimuli-Responsive Functional Materials for Soft Robotics," *Journal of Materials Chemistry B* 8, no. 39 (2020): 8972–8991, <https://doi.org/10.1039/d0tb01585g>.
27. N. Bai, L. Wang, Y. Xue, et al., "Graded Interlocks for Iontronic Pressure Sensors With High Sensitivity and High Linearity Over a Broad Range," *ACS Nano* 16, no. 3 (2022): 4338–4347, <https://doi.org/10.1021/acsnano.1c10535>.
28. R. Yang, A. Dutta, B. Li, et al., "Iontronic Pressure Sensor With High Sensitivity Over Ultra-broad Linear Range Enabled by Laser-Induced Gradient Micro-Pyramids," *Nature Communications* 14, no. 1 (2023): 2907, <https://doi.org/10.1038/s41467-023-38274-2>.
29. Z. Liu, M. Cai, S. Hong, et al., "Data-Driven Inverse Design of Flexible Pressure Sensors," *Proceedings of the National Academy of Sciences* 121, no. 28 (2024): e2320222121, <https://doi.org/10.1073/pnas.2320222121>.
30. K.-H. Ha, H. Huh, Z. Li, and N. Lu, "Soft Capacitive Pressure Sensors: Trends, Challenges, and Perspectives," *ACS Nano* 16, no. 3 (2022): 3442–3448, <https://doi.org/10.1021/acsnano.2c00308>.
31. D. Cafiso, S. Lantean, C. F. Pirri, and L. Beccai, "Soft Mechano-sensing via 3D Printing: A Review," *Advanced Intelligent Systems* 5, no. 6 (2023): 2200373, <https://doi.org/10.1002/aisy.202200373>.
32. H. Li, R. Luo, J. Hu, S. Zhou, X. Zhou, and B. Du, "Lightweight, Elastic and Conductive Pure PEDOT:PSS Foam for Dual-Mode Sensing," *Journal of Materials Chemistry A* 12, no. 25 (2024): 15290–15299, <https://doi.org/10.1039/d4ta01631a>.
33. B. Zhu, J. Guo, W. Li, et al., "Integrated Electromechanical Structure for Iontronic Pressure Sensors With Linear High-Sensitivity Response and Robust Sensing Stability," *Advanced Functional Materials* 34, no. 42 (2024): 2406762, <https://doi.org/10.1002/adfm.202406762>.
34. K. H. Ha, W. Zhang, H. Jang, et al., "Highly Sensitive Capacitive Pressure Sensors Over a Wide Pressure Range Enabled by the Hybrid Responses of a Highly Porous Nanocomposite," *Advanced Materials* 33, no. 48 (2021): 2103320, <https://doi.org/10.1002/adma.202103320>.
35. X. Huang, W. Guo, S. Liu, et al., "Flexible Mechanical Meta-materials Enabled Electronic Skin for Real-Time Detection of Unstable Grasping in Robotic Manipulation," *Advanced Functional Materials* 32, no. 23 (2022): 2109109, <https://doi.org/10.1002/adfm.202109109>.
36. A. Berman, K. Hsiao, S. E. Root, et al., "Additively Manufactured Micro-Lattice Dielectrics for Multiaxial Capacitive Sensors," *Science Advances* 10, no. 40 (2024): eadq8866, <https://doi.org/10.1126/sciadv.adq8866>.
37. X. He, B. Zhang, Q. Liu, et al., "Highly Conductive and Stretchable Nanostructured Ionogels for 3D Printing Capacitive Sensors With Superior Performance," *Nature Communications* 15, no. 1 (2024): 6431, <https://doi.org/10.1038/s41467-024-50797-w>.
38. L. Wu, X. Li, J. Choi, et al., "Beetle-Inspired Gradient Slant Structures for Capacitive Pressure Sensor With a Broad Linear Response Range," *Advanced Functional Materials* 34, no. 26 (2024): 2312370, <https://doi.org/10.1002/adfm.202312370>.
39. X. H. Guo, J. J. Zhao, B. Hu, et al., "Flexible Pressure Sensor With High Sensitivity and Fast Response Based on Bionic Honeycomb-Structured Polydimethylsiloxane/Aluminum Oxide Composites Dielectric via 3-D Printing," *IEEE Transactions on Electron Devices* 71, no. 7 (2024): 4283–4291, <https://doi.org/10.1109/Ted.2024.3401653>.
40. J. Yang, Z. Li, Y. Wu, et al., "Non-Equilibrium Compression Achieving High Sensitivity and Linearity for Iontronic Pressure Sensors," *Science Bulletin* 69, no. 14 (2024): 2221–2230, <https://doi.org/10.1016/j.scib.2024.05.001>.
41. S. Lu, T. Nie, Y. Li, et al., "A Highly Sensitive Flexible Pressure Sensor Based on Inter-Comb Structured Graphene Electrodes," *IEEE Transactions on Electron Devices* 70, no. 4 (2023): 1865–1870, <https://doi.org/10.1109/ted.2023.3248000>.

42. C. Y. Lv, C. C. Tian, J. S. Jiang, et al., "Ultrasensitive Linear Capacitive Pressure Sensor With Wrinkled Microstructures for Tactile Perception," *Advanced Science* 10, no. 14 (2023): 2206807, <https://doi.org/10.1002/advs.202206807>.
43. N. M. Borodachev, "Impression of a Punch With a Flat Square Base Into an Elastic Half-Space," *International Applied Mechanics* 35, no. 10 (1999): 989–994, <https://doi.org/10.1007/bf02682309>.
44. Y. Tanimoto, H. Takechi, H. Nagahata, and H. Yamamoto, "The Study of Pressure Distribution in Sitting Position on Cushions for Patient With SCI (Spinal Cord Injury)," *IEEE Transactions on Instrumentation and Measurement* 47, no. 5 (1998): 1239–1243, <https://doi.org/10.1109/19.746590>.
45. H. Yoon, J.-H. Kim, D. Sadat, A. Barrett, S. H. Ko, and C. Dagdeviren, "Decoding Tissue Biomechanics Using Conformable Electronic Devices," *Nature Reviews Materials* 10, no. 1 (2024): 4–27, <https://doi.org/10.1038/s41578-024-00729-3>.
46. J. Chen, K. Peng, Y. Yang, Y. Dai, B. Huang, and X. Chen, "Hierarchical Iontronic Flexible Sensor With High Sensitivity Over Ultrabroad Range Enabled by Equilibration of Microstructural Compressibility and Stability," *ACS Sensors* 10, no. 2 (2025): 921–931, <https://doi.org/10.1021/acssensors.4c02684>.
47. J. Li, J. Lu, K. Zhang, et al., "Freeze-Drying Induced Gradient Microporous Composite Film With High Ionic Conductivity for Ultrasensitive Wearable Iontronic Pressure Sensor," *Chemical Engineering Journal* 493 (2024): 152450, <https://doi.org/10.1016/j.cej.2024.152450>.
48. Y. Liu, S. Shen, Z. Duan, J. Deng, and D. Fan, "Hydrogels for Long-Term Moisture Retention Under Ambient Conditions: Inhibiting the Evaporation of Free Water From Macroscopic to Molecular Scales," *Advanced Functional Materials* (2025): 2504356, <https://doi.org/10.1002/adfm.202504356>.
49. H. Moeinnia, D. J. Agron, C. Ganzert, L. Schubert, and W. S. Kim, "Wireless Pressure Monitoring System Utilizing a 3D-Printed Origami Pressure Sensor Array," *npj Flexible Electronics* 8, no. 1 (2024): 21, <https://doi.org/10.1038/s41528-024-00309-z>.
50. J. Li, J. Cao, R. Bian, et al., "Multimaterial Cryogenic Printing of Three-Dimensional Soft Hydrogel Machines," *Nature Communications* 16, no. 1 (2025): 185, <https://doi.org/10.1038/s41467-024-55323-6>.

### Supporting Information

Additional supporting information can be found online in the Supporting Information section.

**Supporting Information S1:** smb270002-sup-0001-suppl-data.docx.

**Video S1:** Fabrication process of soft 3DL sensors. **Video S2:** Soft 3DL sensors for signal tracking based on tactile input. **Video S3:** Wearable robotic teleoperation based on soft 3DL sensors. **Video S4:** Soft 3DL sensors as an intelligent robotic fingertip.